Utrecht University

BACHELOR THESIS

Feasibility study for the measurement of the B-meson nuclear modification factor via displaced D mesons with the ALICE detector at the LHC

Eline van der Meer
student number 4174038

January 18, 2017

Institute for Subatomic Physics

Supervisors
Dr. Alessandro Grelli
Dr. André Mischke

Abstract

The universe is believed to have been in a state of free quarks right after the big bang. This state, called a quark-gluon plasma, is subject to many studies as it teaches us about the earliest properties of the universe. The Large Hadron Collider is a particle accelerator built to simulate the quark-gluon plasma phase. Its detectors measure the properties of mesons traversing the quark-gluon plasma. Qualitative comparison of the properties of these mesons to similar mesons that have not traversed a quark-gluon plasma, provides information about the plasma.

In the near future, the LHC will run at an energy of 14 TeV. To make recommendations for this upgrade, simulations in this research have been done at an energy of 14 TeV. Simulations of proton-proton collisions have been made using event generator PYTHIA. The decay $b \to B^0 \to D^{*+}\pi \to D^0\pi\pi \to K^-\pi\pi\pi$ is the decay focused on. Appropriate cuts are investigated based on purity and decay length of the D^{*+} by comparing properties of prompt D^{*+} to that of non-prompt D^{*+}. It is found that the purity of non-prompt D^{*+} is improved to 10% when cutting at $p_T = 12$. The purity of non-prompt D^{*+} can also be improved by making a cut at $p_T = 6$ including a cut at a decay length of 2250 μm, conserving 10% of the original D^{*+}. Recommendations for filtering kaons, which are the mesons that are actually detected by ALICE detectors, by decay length are also made.

Contents

1 Theoretical introduction **3**
- 1.1 Quarks and the Standard Model . . . 3
- 1.2 Quantum Chromodynamics . . . 4
- 1.3 Quark-gluon plasma . . . 5
- 1.4 Heavy quarks and energy loss . . . 7
- 1.5 Nuclear modification factor . . . 9

2 Experimental setup **10**
- 2.1 Large Hadron Collider (LHC) . . . 10
- 2.2 A Large Ion Collider Experiment (ALICE) . . . 11
- 2.3 Time Projection Chamber . . . 12
- 2.4 Time of Flight . . . 13

3 Simulation **14**
- 3.1 PYTHIA . . . 14
- 3.2 ROOT and AliRoot . . . 14

4 Feasibility study for the measurement of displaced D mesons **16**
- 4.1 Objectives of the study . . . 16
- 4.2 PYTHIA configuration . . . 17
- 4.3 Simulation and analysis . . . 18
  - 4.3.1 Purity . . . 24
  - 4.3.2 Decay length . . . 28

5 Conclusions **35**
- 5.1 Outlook . . . 35

A Appendix: Tables of D^{*+} yield **39**

B Appendix: Tables of K^- yield **44**

1 Theoretical introduction

1.1 Quarks and the Standard Model

The ordinary matter on earth is composed of atoms. All atoms have a characteristic nucleus formed by positively charged protons and neutrally charged neutrons. Both of these nucleons consist of three quarks, which are the fundamental particles. Quarks come in six flavors: the positively charged up (u), charm (c) and top (t) and the negatively charged down (d), strange (s) and beauty (b). Each quark flavor has its own antiparticle denoted by a bar on the corresponding quark type ($\bar{u}$, $\bar{d}$). The quark content of a proton is uud and the that of a neutron is udd. The proton and neutron are examples of hadrons, which are particles that consist of quarks. Particles made of three quarks are called baryons and particles made of a quark and an antiquark are called mesons.

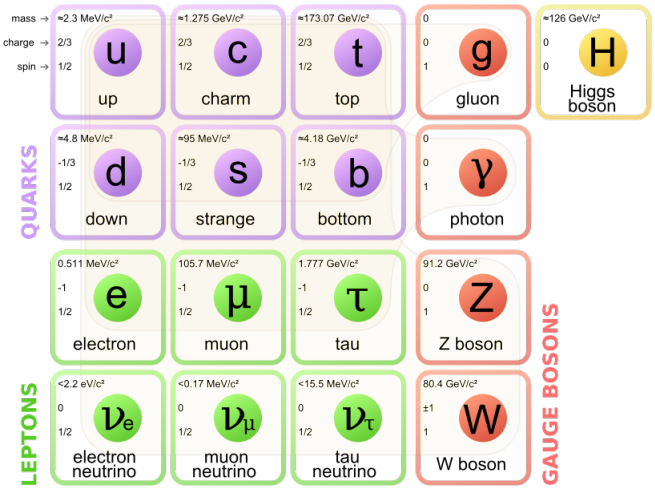

Figure 1: Elementary particles in the Standard Model [1]

The behavior of quarks is described in the Standard Model. This is currently the scientifically accepted model that describes properties of particles and their interactions. The Standard Model divides all elementary particles into fermions, of which matter is made up, and bosons, which can be seen as the glue holding the fermions together. The fermions are characterized by

their half-integer spin and can be classified into quarks and leptons.

The Standard Model describes how leptons interact through the electromagnetic and the weak force, while the quarks interact through the strong, electromagnetic and weak force. Quantum Chromodynamics is the theory describing the strong interaction between quarks and gluons [2].

1.2 Quantum Chromodynamics

Quarks have not been observed freely. They are held together within hadrons by the strong force. Quantum Chromodynamics (QCD) is the theory describing this strong interaction between quarks and gluons. Quantum electrodynamics (QED) describes how particles exchange electrical charge through photons.

Quantum Chromodynamics shows similarities to quantum electrodynamics. QCD implies that quarks carry color charge, analogous to how matter carries electrical charge in QED. Quarks carry the color charge red, blue or green and antiquarks carry antired, antiblue and antigreen. The color charge of a quark represents how strongly a particle interacts with the strong force field. Only color neutral particles have been observed: both mesons with one color and its anticolor and baryons with three different colored quarks make for colorless particles.

There is one considerable difference between QED and QCD theory that concerns the force carriers. Photons are the force carriers of electrical charge, gluons are the force carriers of color charge. According to QED, photons do not carry electrical charge but merely transfer it from one particle to another. Gluons, force carriers of the strong force, however, are color charged themselves. This means gluons are able to interact with both quarks and each other which leads to a strong dependence on momentum transfer in the coupling constant.

This coupling constant describes the strength of the force in a strong interaction. At high momentum or short distance, the coupling constant for strong interactions α_s is described by a single coupling constant as is the case in electroweak theory [2].

$$\alpha_s(Q^2) = \frac{\alpha_s(\mu^2)}{1 + \beta_0 \alpha_s(\mu^2) ln(Q^2/\mu^2)} \tag{1}$$

$$where \;\; \beta_0 = \frac{11N_c - 2n_f}{12\pi}$$

$$N_c = number\ of\ colours$$

$$n_f = number\ of\ flavours$$

$$Q = exchanged\ four - momentum$$

$$\mu = constant$$

The dependence on the squared exchange of four-momentum illustrates that the strength holding quarks together gets weaker as the distance between them decreases. As the distance between quarks increases, the strong force increases as well. This phenomenon can be explained by the gluons that carry color charge: the greater the distance the quarks interact at, the more gluons are contributing to this interaction, resulting in a greater coupling. This implies that at infinitely small distances, quarks do not experience the strong force enabling them to move freely. This is called asymptotic freedom. Asymptotic freedom can also be reached when quarks interact at extremely high energies. The latter is important to our research, as we reconstruct asymptotically free quarks through collisions at very high energies. The asymptotically free quarks form a matter of unconfined particles called the quark-gluon plasma.

1.3 Quark-gluon plasma

Quark-gluon plasma (QGP) is a phase transition quarks and gluons can be in for a very short time under the restriction of very high temperature and

density. This is believed to be the state the universe was in several microseconds after the Big Bang. After a very short time of existence the QGP cooled down, confining the free quarks in hadrons, forming the hadronic matter as we know it today [4].

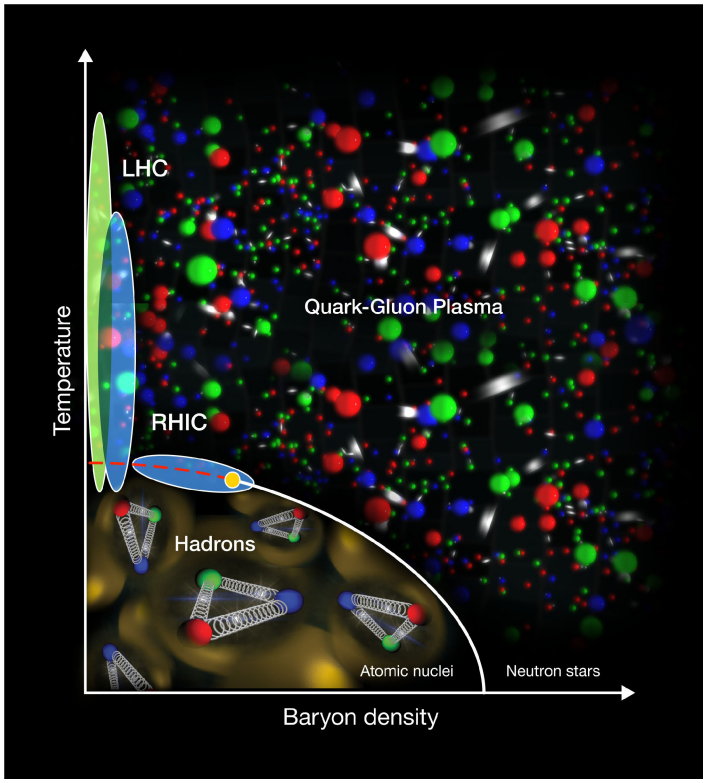

Figure 2: Quark-gluon plasma is formed at high particle density and high temperature [5].

Studying the properties of the QGP means learning about the earliest conditions of the universe right after it was created. The QGP however cannot be studied directly, as its time of existence is approximately 10^{-23} s, which is too short to be measured directly. Hence we need a probe to go through the QGP and measure it after it traveled through the QGP. A certain probe that can be used for this purpose, is a heavy quark that is produced the moment the two heavy ions collide. At the time of collision, two important things happen. First of all, heavy quark pairs are formed by either colliding gluons

or colliding (lighter) quarks that are confined within hadrons. Consequently, the temperature gets high enough for the QGP to form. The heavy quarks can thus be used as probes traveling through the QGP. It is important for our study that the probe travels through the complete plasma. For this purpose charm and beauty quarks are of use.

The QGP is formed by heating matter to temperatures higher than $2 * 10^{12}$ K [6]. This makes the QGP the hottest structure to have ever been created on earth. It is created at the Large Hadron Collider. The production of QGP is facilitated by colliding two heavy nuclei. At the LHC, this is done by colliding two lead ions. The heavy ions are accelerated to relativistic speeds and energies in the order of 10^{12} eV so that in the event of a collision a quark-gluon plasma is formed.

1.4 Heavy quarks and energy loss

After quarks have traversed the QGP as described in the previous section, they decay into measurable mesons. Properties of these mesons like their momentum and angle of propagation provide information about the QGP. In order for these measurable mesons to be formed, the quarks need to have traveled through the plasma completely. Some quarks annihilate before they have traveled through the plasma completely due to energy loss. They lose energy through the gluons they emit. They emit gluons in a radius

$$\theta > \frac{m_q}{E_q},$$

which shows the proportionality of the mass of a quark to the gluon radiation angle. Lighter quarks emit more gluons than heavy quarks, as for heavy quarks gluon radiation within the angle $\theta < m_q/E_q$ is suppressed more. This is called the dead-cone effect [6].

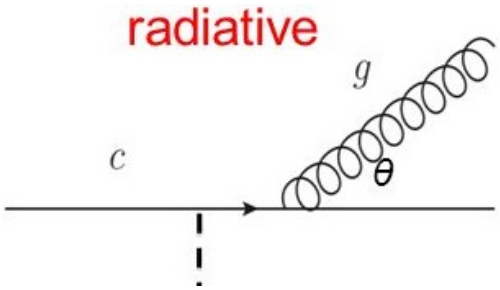

Figure 3: Feynman diagram of gluon radiation [7].

Therefore, heavy quarks lose less energy traversing the QGP and are more likely to come out of the plasma and hadronize into mesons. As can be seen in table 1, the top quark t is the heaviest quark. It is also the fastest decaying quark, causing it to decay before it has traveled through the plasma completely. Charm quark c and beauty quark b are the next most massive quarks, and their lifetimes allow for them to travel through the plasma completely before decaying into mesons. Charm quarks hadronize into D mesons, beauty quarks into B mesons. These mesons decay into kaons and pions, which are detectable particles.

Quark flavor	Mass ($\frac{MeV}{c^2}$)
u	3
d	6
c	1300
s	110
t	180000
b	4200

Table 1: Quark masses [2].

1.5 Nuclear modification factor

Now, we have suitable meson-candidates for investigation of the quark-gluon plasma: kaons and pions originating from charm and beauty quarks. To obtain actual information about the QGP, we need to do measurements on these same mesons that have decayed from charm and beauty quarks that did not travel through a QGP. To this end we will investigate proton-proton collisions. Proton-proton collisions can be seen as a scaled-down version of the lead-lead collisions, the most significant difference being that no QGP is produced in proton-proton collisions. Therefore, the charm and beauty quarks produced in proton-proton collisions will not have traversed a QGP. The mesons they decay into are similar to those the quarks in lead-lead collisions decay into. The nuclear modification factor R_{AA} defined as

$$R_{AA} = \frac{1}{N} \frac{dN/dp_t(PbPb)}{dN/dp_t(PP)} \tag{2}$$

can give us information about the quark-gluon plasma. It is the ratio of particle yield in lead-lead collisions and the particle yield in proton-proton collisions, corrected by a normalization factor N. This corrects for the fact that a lead nucleus consists of multiple protons. In the QGP, particles that travel through it will lose energy, causing the relative particle yield in lead-lead collisions to be smaller than the yield in proton-proton collisions. This results in $R_{AA} < 1$ and information about the energy of the quark-gluon plasma.

2 Experimental setup

The collisions we simulate are done in real life at the European Organization for Nuclear Research (CERN) in Switzerland and France. Particle accelerators like the Large Hadron Collider (LHC) and detectors like ALICE are used to perform heavy-ion experiments. In this section, the accelerators and detectors relevant to our research will be discussed.

2.1 Large Hadron Collider (LHC)

The Large Hadron Collider is the world's largest particle accelerator. It was built by CERN between 1998 and 2008. It is located next to Geneva just across the French border. The accelerator is a 27 kilometer long tunnel built underground. The tunnel houses two parallel beam pipes. The two particle beams travel in opposite directions through the circular construction. The beam pipes are designed to accelerate and collide protons and heavier nucleons like lead ions. The first runs of the LHC in 2009 were at an energy level of 1.18 TeV per beam, making it the world's highest energy particle accelerator. After that, the energy levels have been ramped up, until in 2013 the LHC was shut down for a large-scale upgrade. In 2015 it was restarted and ran proton-proton collisions at a total energy of 13 TeV (6.5 TeV per beam). The LHC is planned to run at an energy of 14 TeV in 2018.

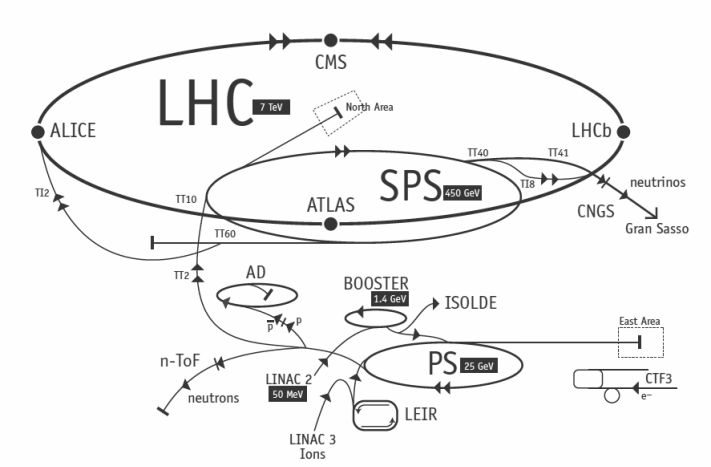

Figure 4: Schematic view of the LHC including its detectors [8].

Seven detectors have been built at LHC to detect the particles that emerge at the collisions: ATLAS, CMS, LHCb, ALICE, and three smaller, more specialized detectors. ATLAS is a general particle detector used for research on expanding the Standard Model. CMS searches for dark matter and the Higgs boson. LHCb performs measurements on charge parity violation. The ALICE detector was designed for investigation of the quark-gluon plasma and is the detector that is relevant for our research.

2.2 A Large Ion Collider Experiment (ALICE)

ALICE is a heavy-ion experiment that focuses on investigating the quark-gluon plasma. It is one of the detectors in the LHC and is built to run lead-lead collisions at center of mass energies of 2.76 TeV. This energy level is high enough to produce quark-gluon plasma in the collision.

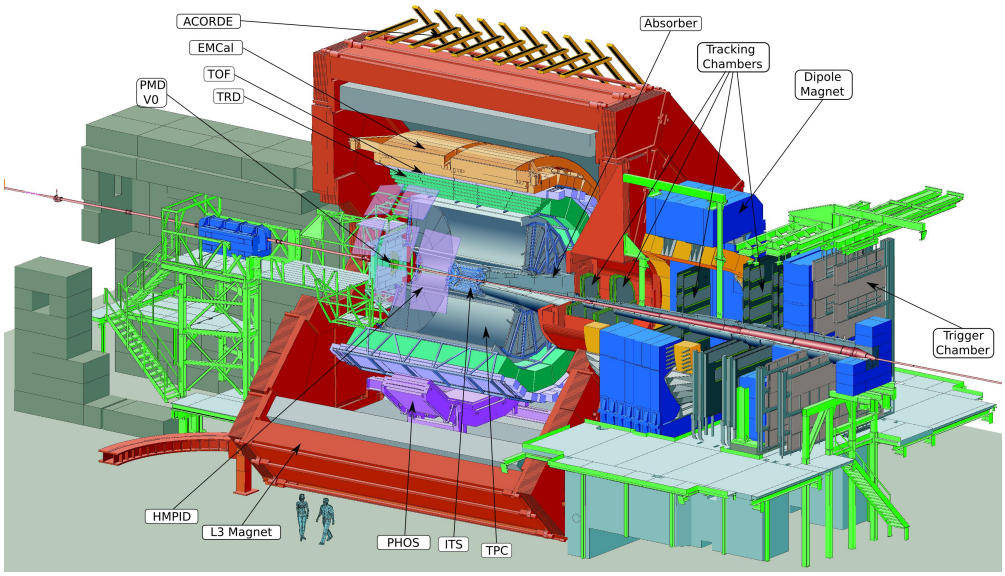

Figure 5: Sketch of the ALICE experiment and its detectors [8].

ALICE is able to detect particles that are created in the hot QGP and that live long enough to reach the detectors. To this end it has 18 built in detectors. In figure 5, a schematic view of ALICE is depicted. The main collision point is surrounded by cylindrical barrel detectors that detect the out flying particles. These barrel detectors reside in a magnetic field, causing the

trajectories of the particles to bend which enables the trackers to determine their momenta. Particles can be detected within an angle of $\eta < 0.9$, η being the pseudorapity which is the angle of a particle with respect to the particle beam. A value of $\eta = 0.9$ corresponds to roughly 45°. From the central point of interaction outwards the particles encounter the Inner Tracking System (ITS), Time Projection Chamber (TPC) and the Time Of Flight (TOF) detectors.

The ITS aims to measure the heavy particles before they decay. It measures the particles with precision of a tenth of a millimeter [9]. It consists of three layers of detectors. This tracking system is relevant for our research as it identifies particles containing charm and beauty quarks by determining their decay vertices.

2.3 Time Projection Chamber

The main particle tracker of ALICE is the Time Projection Chamber (TPC). The TPC surrounds the ITS as shown in figure 6. It uses a combination of electric fields, magnetic fields and $Ne - CO_2$ gas to reconstruct the trajectories of particles in 3D. The volume of the gas is 88 m^3.

When charged particles travel through the $Ne - CO_2$ gas, they ionize the this gas. This frees electrons from the gas, which drift towards the cylindrical plates of the TPC. The electrical signal the electrons give is amplified and simultaneously, positive ions that drift in the gas chamber induce a positive electrical field. This signal is consequently read by the cathode pads located at the end of the TPC. The TPC is suitable for reading out signals from heavy-ion collisions, as it is able to detect large numbers of particles simultaneously.

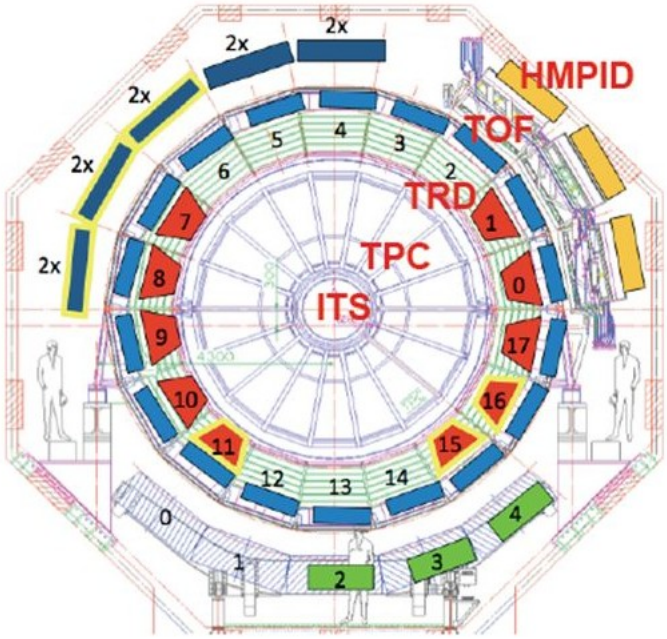

Figure 6: Cross section of the inner ALICE detectors [10].

2.4 Time of Flight

The TPC is able to determine the charge and momentum of a produced particle. To identify a particle the velocity of it also has to be known: then the mass of the particle can be computed by the measured momenta and velocity. To this end the TPC collaborates with the Time of Flight (TOF) detector. It measures the time a particle needs to travel from its production vertex to the detector, from which the velocity of the particle can be determined.

The TOF detector is located 3.7 m from the beam pipes. It has a cylindrical surface of 150 m^2 which is covered in multigap resistive plate chambers. 160.000 MRPC plates are placed with a small spacing between them for optimal detector accuracy. This results in the TOF being able to measure flight time with a precision of 10^{-13} s [11].

3 Simulation

This research will consist of computer simulations made with the software ROOT and PYTHIA. To simulate collisions as they take place at the LHC and analyze them, we used the computer software PYTHIA, ROOT and AliRoot. Since these simulations are based on real data obtained at the LHC, these can provide us with helpful information about future real-life experiments.

3.1 PYTHIA

PYTHIA is an event generator that combines QCD theory and data obtained in particle collision experiments. It is a Monte Carlo simulator, meaning that it applies repeated random sampling to replicate realistic randomness in particle experiments. PYTHIA can generate proton-proton collisions as well as heavy-ion collisions like lead-lead collisions. From these collisions PYTHIA generates the particles that will be produced. Next to that, it does not have the physical limitations the actual detectors have as described in the section above. For example, it can list particles in the full pseudorapity η range. By comparing this to a scenario where the $\eta < 0.9$ condition has been met, we can compute how much of the particles in an interaction are actually detected.

In this study version PYTHIA 8.1 created by Lund University [12] has been used. This version of PYTHIA has been rewritten completely in C^{++}, where older versions of the program were written in Fortran. The simulations done with PYTHIA have been run in the program AliRoot.

3.2 ROOT and AliRoot

ROOT is a framework for data processing. It was developed at CERN in 1994 to analyze data from particle physics experiments [13]. Currently, it is still used for analysis and data acquisition in particle physics due to its high computing efficiency. The program is largely based on C^{++}, making it an imperative and object-oriented coding program. Additional libraries specialized for particle analysis have been incorporated. The histograms in section 3 have been made with ROOT.

AliRoot is the ALICE off line framework for simulations. It uses ROOT as a basis for the AliRoot framework. In this study we used AliRoot to analyze simulations made with PYTHIA. We incorporated PYTHIA in AliRoot and ran the simulations in the quark cluster at the Institute for Subatomic Physics at Utrecht University. This is a server with large computing capability suitable for generating large sets of data.

4 Feasibility study for the measurement of displaced D mesons

4.1 Objectives of the study

Our objective is to obtain a clean sample of B meson decays, that is, the decay

$$b \to B^0 \to D^{*+}\pi \to D^0\pi\pi \to K^-\pi\pi\pi$$

b being the beauty quark. The theoretical branching fraction of beauty quarks decaying into B^0 mesons is $40,2 \pm 0,7\%$ [14].

We will attempt to achieve this through investigating the properties of the D^{*+} meson. This meson is also produced in the decay

$$c \to D^{*+} \to D^0\pi \to K^-\pi\pi$$

c being the charm quark. The D^{*+} coming from a charm quark is called a prompt D^{*+} meson. The theoretical branching fraction of charm quarks decaying into D^{*+} is $25,5 \pm 1,5\%$ [14].

Both of these decays occur in a proton-proton collision and in a lead-lead collision. Hence it is useful to investigate the properties of the D^{*+} when it has traveled through a QGP (in Pb-Pb) and when it has not (in pp).

In this study, we will try to obtain a clean sample of B meson decays using two different methods. First of all, we will look at the transverse momenta p_T of the D^{*+} in both decays starting from a beauty and a charm quark. By dividing the sample we generate in PYTHIA into different p_T-bins and comparing the particle yield in each bin, we can calculate the purity of the sample. Optimized cuts in the momentum distributions can be based on this data analysis. Secondly, the difference in decay length of the $c \to D^{*+}$ track and the $b \to B^0 \to D^{*+}$ track will be inspected. Again per transverse momentum p_T bin the relation of the decay lengths to another will be checked and an optimal cut will be the aim.

4.2 PYTHIA configuration

In this study event generator PYTHIA has been used. This event generator bases its events on real data generated by the LHC, as described in section 2.1. In the configuration, the user can vary the settings so the desired decay can be studied. For our study we have used the following settings:

- System: proton-proton
- Center of mass energy = 14 TeV

The LHC does not yet run at an energy of 14 TeV. This is however anticipated to happen in the future. The simulations done in this study will therefore be a helpful support for future data that will be generated by the LHC.

The B meson decay we are interested in, is a rare track. For rare decays like these, PYTHIA has the possibility to force certain decays to occur. The ratio of particles the beauty quark decays in does not change, which makes it suitable for research. It ensures we need not simulate as many events, yet still have a statistically usable outcome. In the forced configuration of PYTHIA we write:

- HardQCD:gg2bbbar = on
- HardQCD:qqbar2bbbar = on
- Random:setSeed = on

The first two settings force PYTHIA to generate pairs of beauty anti-beauty quarks from both gluons and other quark flavors. This results in more produced beauty anti-beauty pairs than without the forced settings. The last setting is to make sure every simulation runs a different set of random events.

The unforced setting of PYTHIA would be to write

- HardQCD:All = on

instead of the first two forced settings. This setting causes all types of quarks to be generated in a proton-proton collision.

4.3 Simulation and analysis

First of all, we generated proton-proton collisions with the forced beauty settings as described above turned on. In figure 7, we can see the transverse momenta of the charm and beauty quarks produced in proton-proton collisions. Nine million events were simulated in which 943251 charm quarks and anti-quarks were produced and 5833 beauty quarks and anti-quarks. These make for branching ratios of 10.5% produced charm quarks per event and $6.5 * 10^{-2}$ % produced beauty quarks per event.

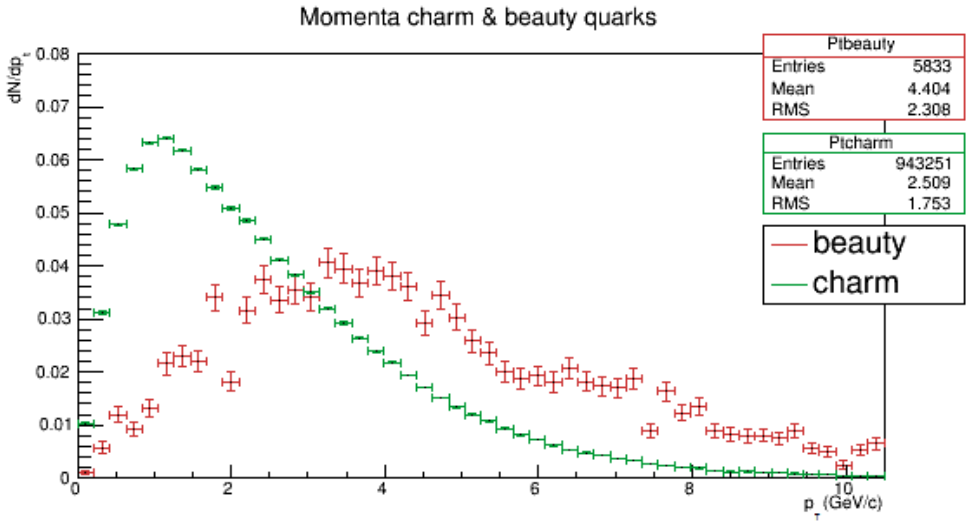

Figure 7: Transverse momenta of charm and beauty quarks, $9 * 10^6$ events, pp at 14 TeV.

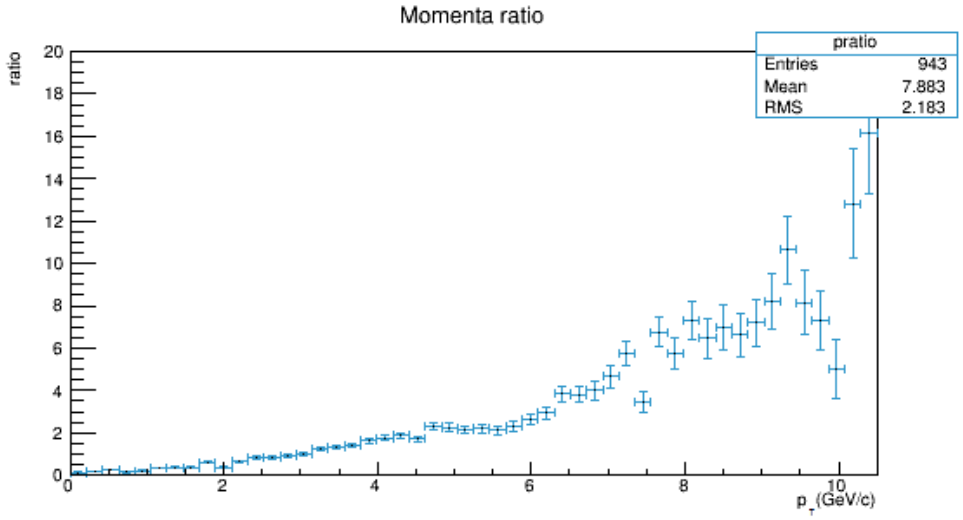

Figure 8: Ratio of the transverse momenta of charm and beauty quarks, $9 * 10^6$ events, pp at 14 TeV.

We can already see the difference in transverse momentum in this figure. The charm quark shows a peak in momenta at 1.2 GeV/c and a mean of 2.5 GeV/c. The beauty quark shows a similar but lower peak at 3.5 GeV/c and has a mean of 4.4 GeV/c. The beauty quark has a higher average momentum than the charm, but the relative particle yield is lower than the charm yield. This indicates that D^{*+} coming from beauty quarks will likely have a higher momentum than prompt D^{*+}.

Figure 8 is a ratio plot defined as $\frac{b_{p_T}}{c_{p_T}}$. It shows that at a momentum of 3.0 GeV/c, the ratio of p_T exceeds 1. This means that at $p_T > 3.0$ GeV/c the relative fraction of beauty quarks exceeds that of charm quarks.

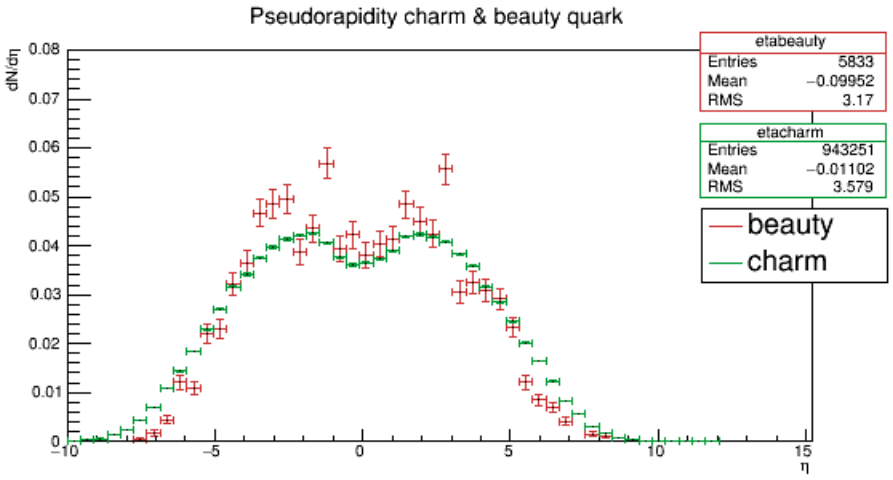

Figure 9: Pseudorapidity of charm and beauty quarks, $9 * 10^6$ events, pp at 14 TeV.

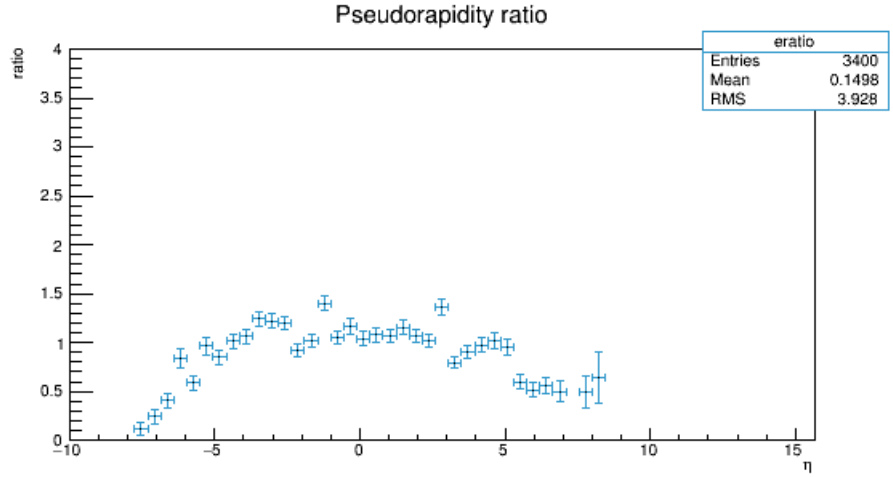

Figure 10: Ratio of pseudorapidity of charm and beauty quarks, $9 * 10^6$ events, pp at 14 TeV.

In figure 9, the pseudorapidity η is illustrated, which is a measure for the angle with respect to the direction of the particle beam. ALICE can measure

up to $\eta = 0.9$, corresponding to an angle of 45° . Figure 9 shows the full range of η, but as this is not the case in the actual particle detection at LHC, further analysis will be done with the constraint of $|\eta| < 0.9$.

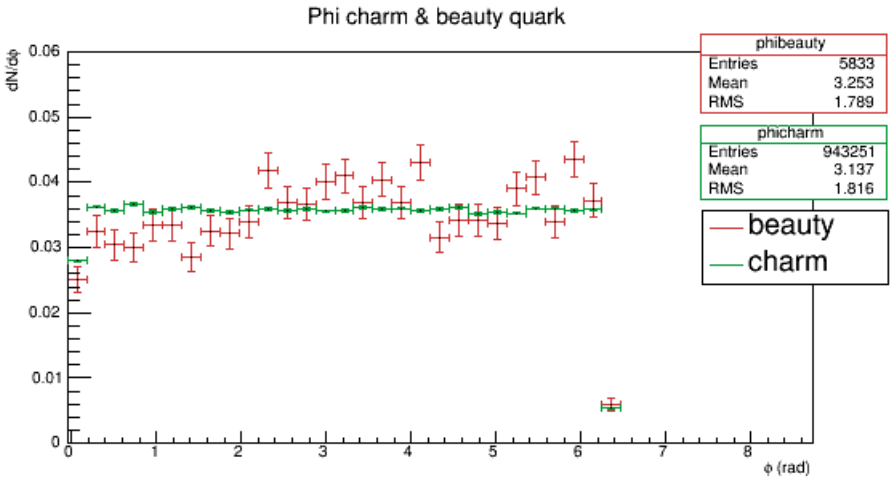

Figure 11: Azimuthal angle ϕ of charm and beauty quarks, $9 * 10^6$ events, pp at 14 TeV.

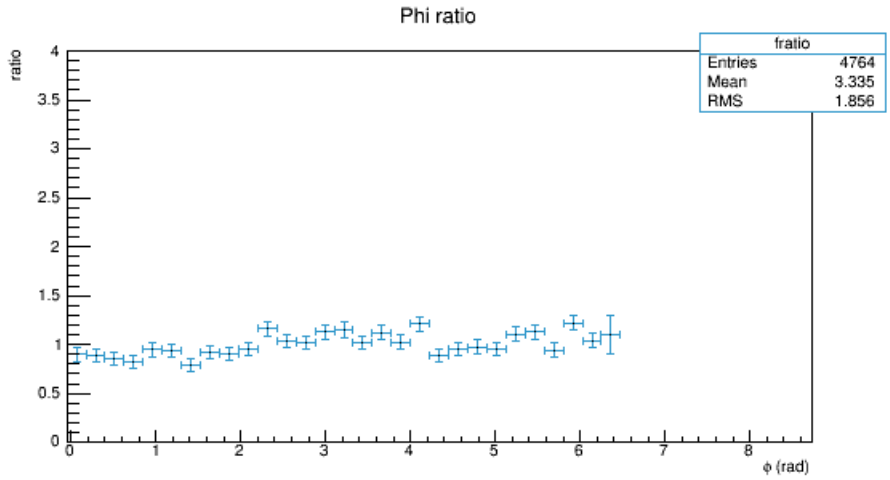

Figure 12: Ratio of ϕ of charm and beauty quarks, $9 * 10^6$ events, pp at 14 TeV.

The azimuthal angle ϕ is covered completely, that is for 2π rad, in the ALICE detector. As we can see in figure 11 the charm quark particle yield is very constant throughout the azimuthal angle ϕ. The beauty particle yield shows slight fluctuations around the constant value of the charm. These graphs indicate that the ϕ measurement of D^{*+} might not be a promising search.

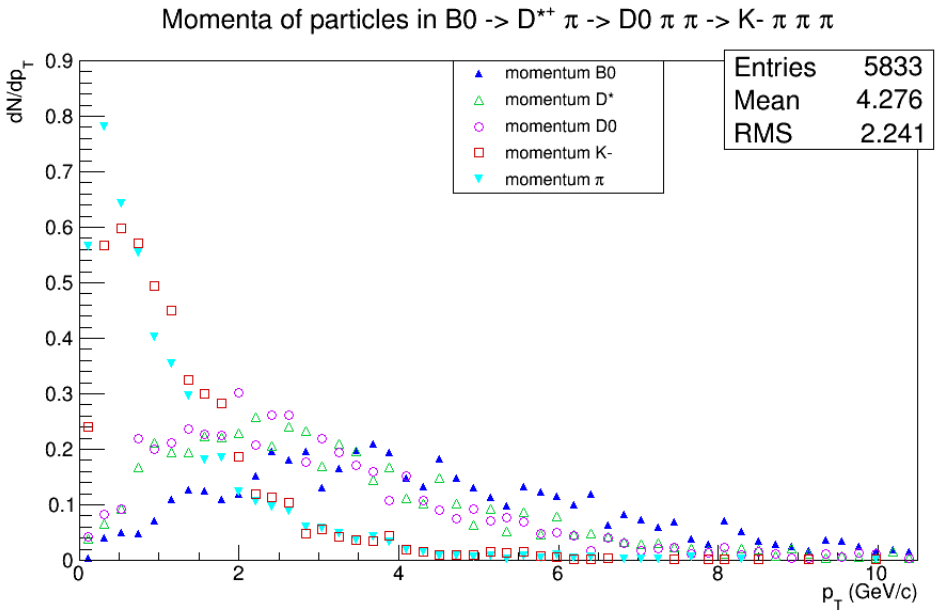

Figure 13: Momentum distributions of decay particles of the B^0, $9 * 10^6$ events, pp at 14 TeV.

The particle track the beauty decays in is given by

$$b \to B^0 \to D^{*+}\pi \to D^0\pi\pi \to K^-\pi\pi\pi$$

All of these particles have transverse momenta which can be computed by PYTHIA. In the ALICE detector, only the final particles K^- and π can be measured. Therefore, it is relevant to construct the p_T of the remaining particles with PYTHIA to get a complete outline of the selected decay. In figure 13 we can see the B^0 has the highest average momentum, followed by respectively the D^{*+}, D^0, K^- and π. This is a logical consequence of the energy loss the particles undergo as they travel a longer distance and decay into other particles.

4.3.1 Purity

To simulate the actual circumstances of the LHC, we will now simulate data with the limitation of $|\eta| < 0.9$. The transverse momenta of the D^{*+} are illustrated in figure 14, both for the situation of η everywhere and $|\eta| < 0.9$.

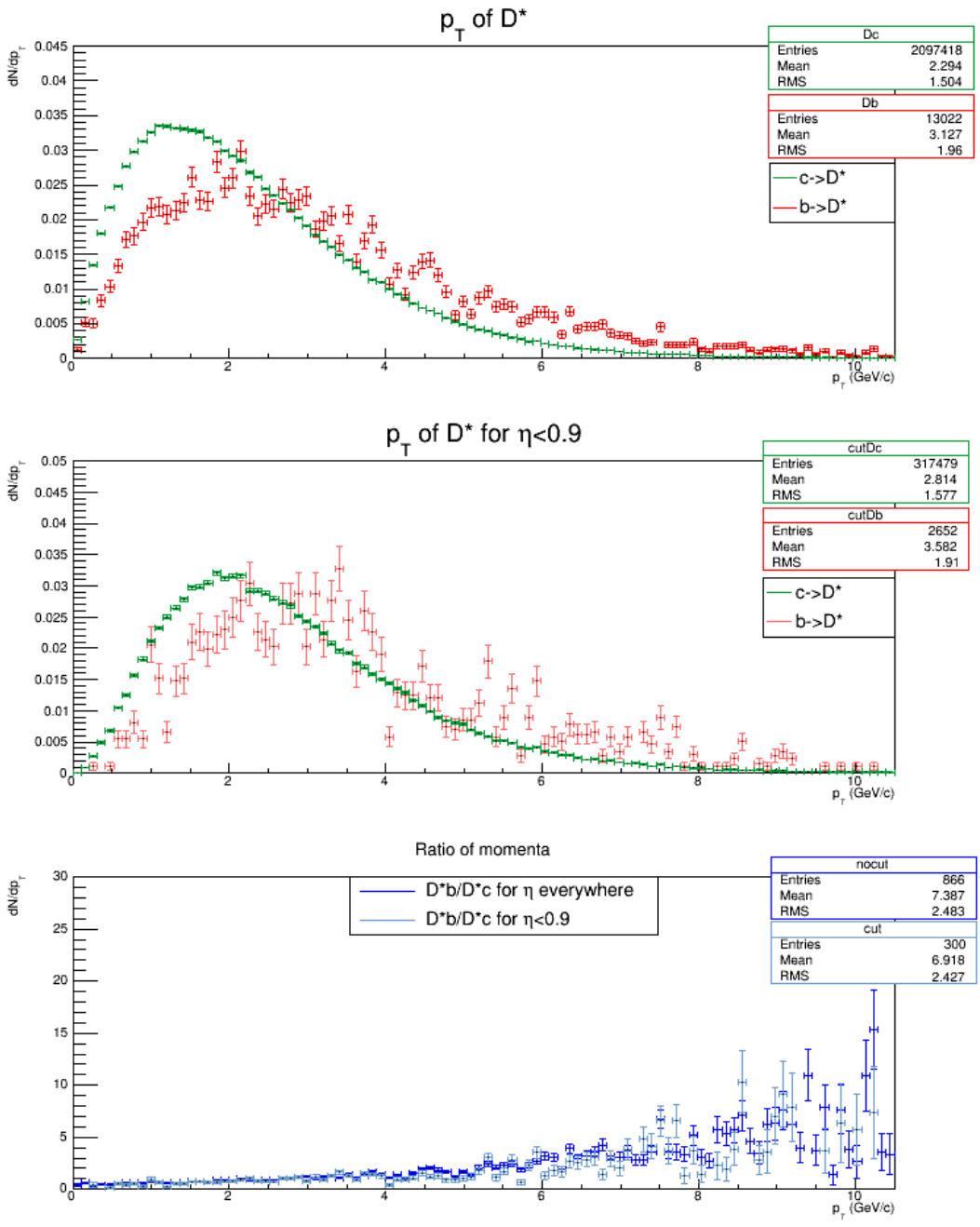

Figure 14: Transverse momentum of D^{*+} for η cut and no cut. $20 * 10^6$ events, pp at 14 TeV.

As anticipated the momentum of the D^{*+} coming from the B^0 meson is higher than the momentum of the prompt D^{*+}. This is most clearly visible in the plot of the uncut η, but also still clear from the plot of the cut η. The uncut η yields a mean transverse momentum value for prompt D^{*+} of $p_T = 1.2$ GeV/c and a value of $p_T = 2.5$ GeV/c for non-prompt D^{*+}. The cut η graph yields a mean transverse momentum value for prompt D^{*+} of $p_T = 1.8$ GeV/c and a value of roughly $p_T = 3$ GeV/c for non-prompt D^{*+}. For a realistic condition of η, on average higher momentum D^{*+} should be measured.

The purity of the D^{*+} coming from B-mesons is defined as

$$P_{D_b^{*+}} = \frac{D_b^{*+}}{D_b^{*+} + D_c^{*+}}.$$

D_b^{*+} being the D^{*+} coming from B-mesons particle yield and D_c^{*+} being the prompt D^{*+} particle yield.

The measurement of the purity $P_{D_b^{*+}}$ is done in several p_T bins with the objective of possible comparison to decay length per p_T bin, as we shall see later in section 4.3.2.

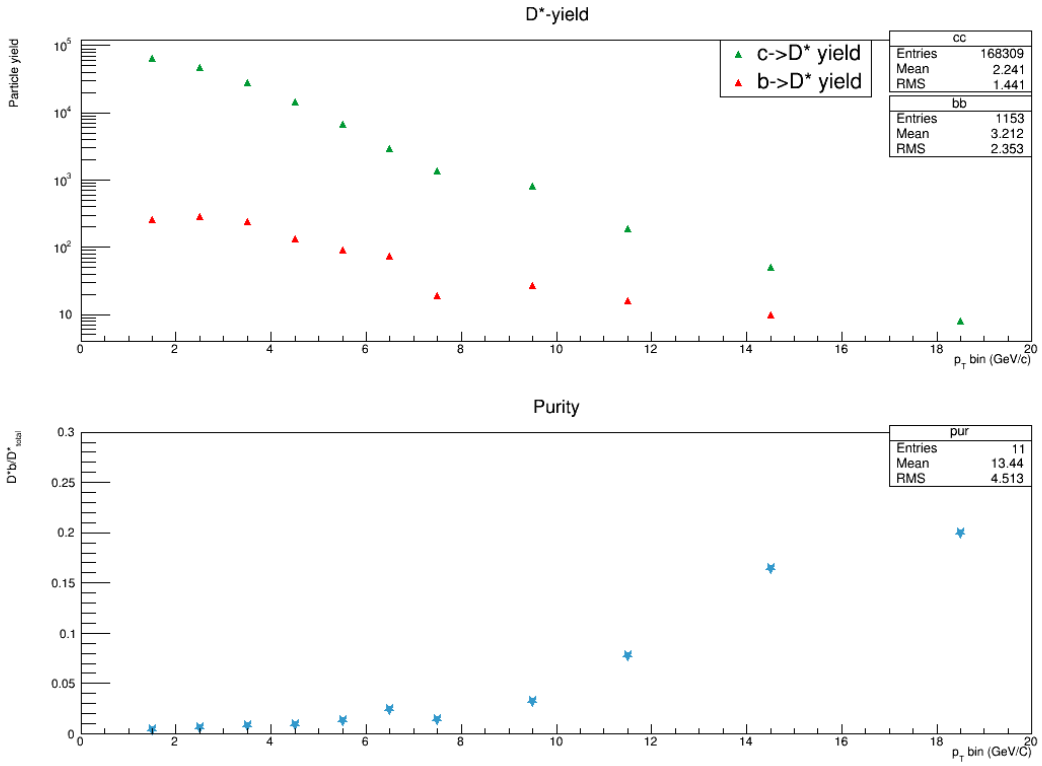

Figure 15: Purity of the D* from beauty. $5 * 10^6$ events, pp at 14 TeV

At higher p_T bins the purity seems to improve more. In the bin $12 < p_T < 16$ it exceeds the value of 0.1, corresponding to a purity of 10 per cent, for the first time. This seems to be a good place to make a cut.

4.3.2 Decay length

Next, we will take a look at the decay length of the D^{*+}. The prompt D^{*+} is expected to have a very short decay length, while the D^{*+} is expected to have traveled a longer distance. The decay length of the D^{*+} as we have measured in this study is the distance between creation of the quark and creation of the daughter of the D^{*+}, in this case the D^0.

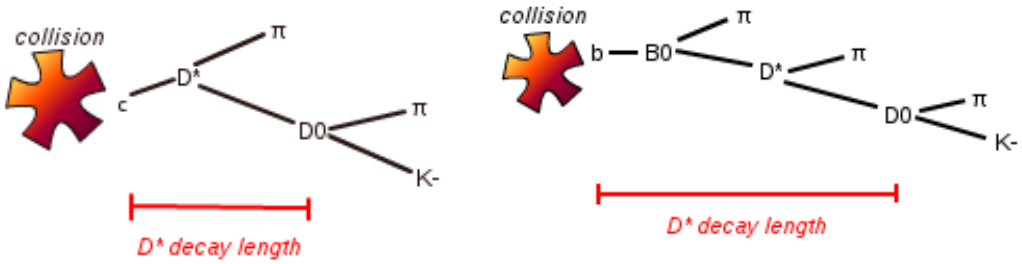

(a) D^{*+} coming from charm

(b) D^{*+} coming from beauty

Figure 16: Illustration of the decay lengths of the D^{*+}

Figure 16 illustrates that the decay length of a D^{*+} coming from beauty is longer than that of a prompt D^{*+}. This has two reasons. First of all, a prompt D^{*+} has only a charm quark as mother particle. A D^{*+} coming from beauty has a B^0 meson as a mother particle, which on its turn has a beauty quark as mother particle. Next to that, the distance from creation of the D^{*+} to creation of a D^0 is very short. The distance however from creation of the B^0 to decay of the B^0 is expected to be much larger. Therefore, we expect a larger decay length of the D^{*+} from beauty than of the prompt D^{*+}.

First, the decay lengths of the D^{*+} in the whole p_T region were simulated. Again the $|\eta| < 0.9$ cut was made for detection purposes. As can be seen in figure 17 the decay length of the prompt D^{*+} is even smaller than expected: it is nearly negligible. On 15 million entries, the average decay length is 0 μm.

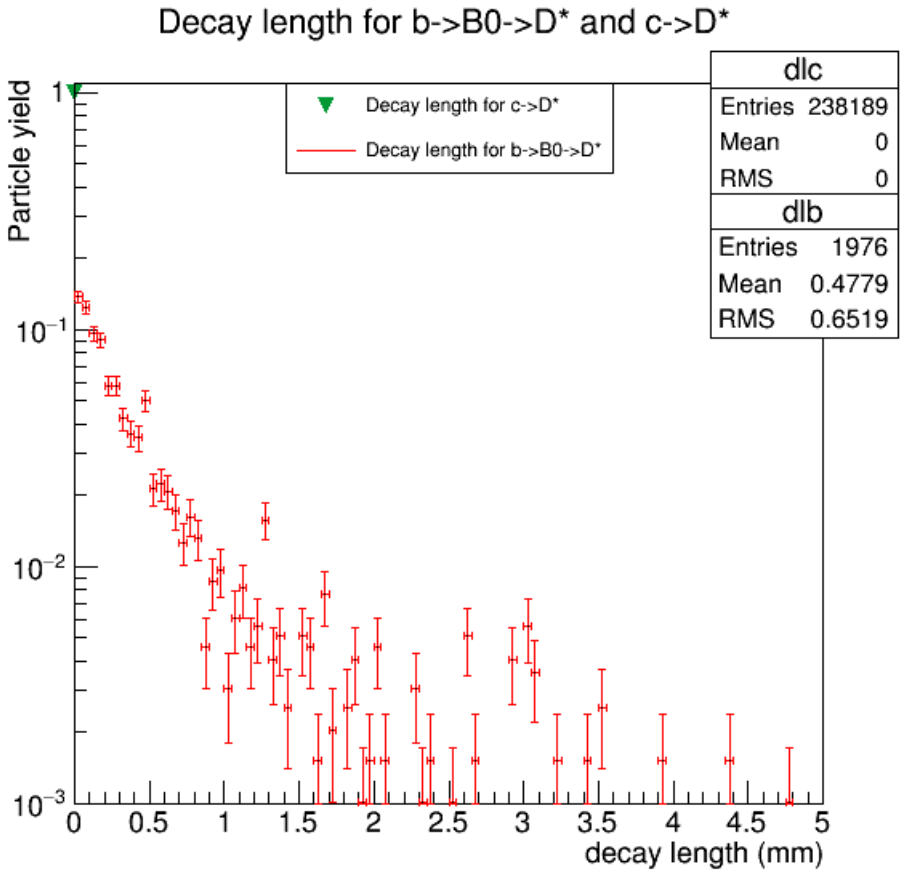

Figure 17: Decay length D* from charm and beauty. $15 * 10^6$ events, pp at 14 TeV.

In figure 18, the decay lengths of the D^{*+} per p_T bin are depicted. From the data in the upper row we can see that the curve of the decay length of the D^{*+} from beauty seems to decrease in steepness for increasing momentum. The data in the lower row are statistically too little to give information.

The decay length of the prompt D^{*+} stays at a steady negligible distance for each p_T bin.

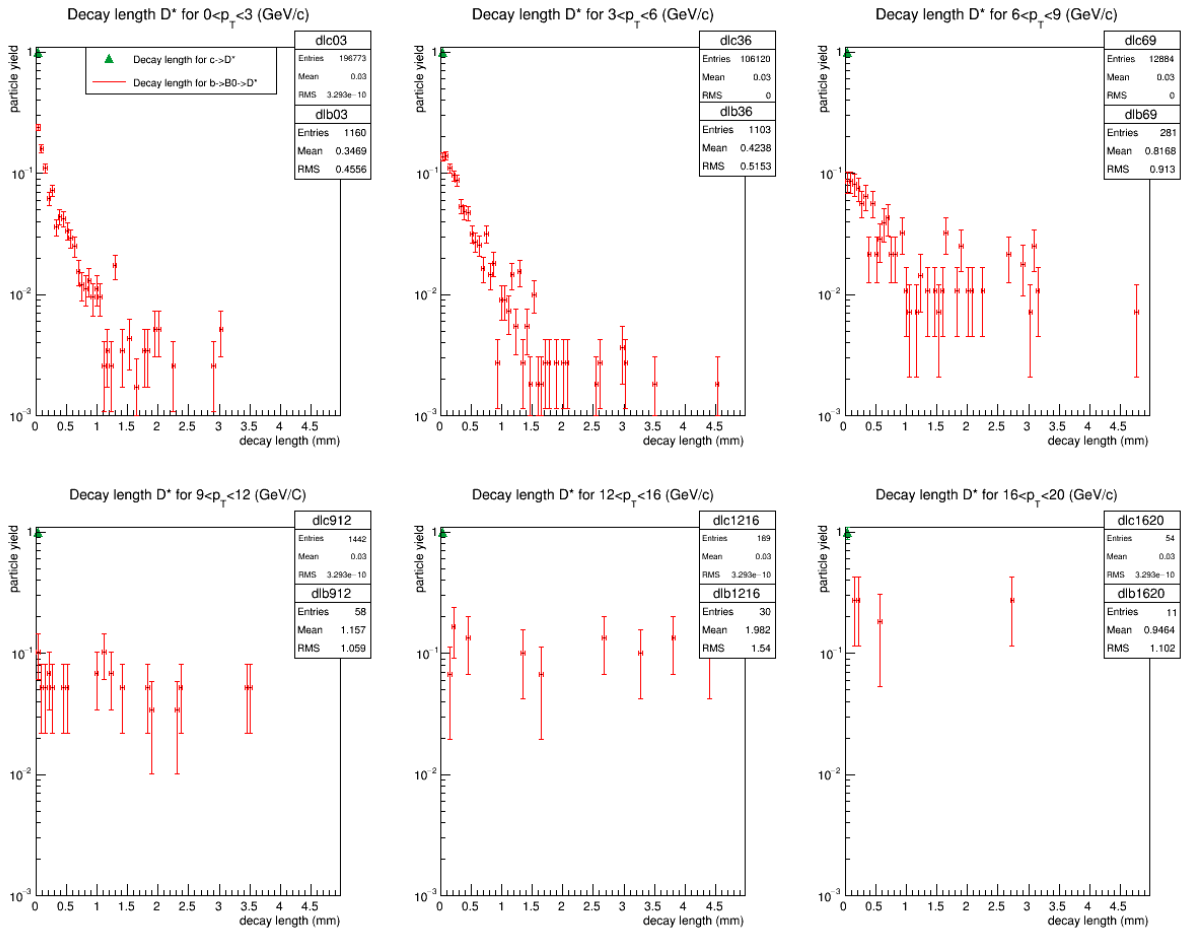

Figure 18: Decay lengths of the D^{*+} per p_T bin. $20 * 10^6$ events, pp at 14 TeV.

Tables of the particle yield of the D^{*+} can be found in Appendix A. These

are data abstracted from figure 18. Per p_T bin, the number of non-prompt D^{*+} that decay at a certain length is counted and the percentage this is of the total non-prompt D^{*+} yield is given. A summary of these tables is given in figure 2. To get a sample where 10% of the non-prompt D^{*+} are left within the p_T range $0 < p_T < 3$ GeV/c, a cut would have to be made at 850 μm, meaning all data of D^{*+} that have a shorter decay length than 850 μm are discarded.

p_T **bin**	D^{*+} **left at decay length (μm)**		
	10%	**30%**	**50%**
$0 < p_T < 3$ GeV/c	850	350	150
$3 < p_T < 6$ GeV/c	1050	550	250
$6 < p_T < 9$ GeV/c	2250	950	450
$9 < p_T < 12$ GeV/c	3450	1350	1050
$12 < p_T < 16$ GeV/c	4350	3250	1650
$16 < p_T < 20$ GeV/c	2750	550	250

Table 2: Percentages of D^{*+} left after making a cut.

It would be sensible to make a cut at a decay length > 1000 μm for detector accuracy purposes. The p_T regions that satisfy this condition are $p_T > 6$. Since the regions $16 < p_T < 20$ GeV/c, $12 < p_T < 16$ GeV/c and $9 < p_T < 12$ GeV/c produced little data ($\sim 10^1$ D^{*+} in $20 * 10^6$ million events), it would be advisable to focus on the region $6 < p_T < 9$ GeV/c which has a combination of a bigger sample and a relatively large decay length at which a cut can be made.

Similar data regarding decay length has been generated for K^-. This is a measurable particle in the ALICE detectors and therefore very relevant to research. In figure 19, the decay lengths of the kaons are depicted per p_T bin. In the lower p_T areas it can be seen how kaons coming from charm quarks decay at a shorter length than kaons coming from beauty quarks.

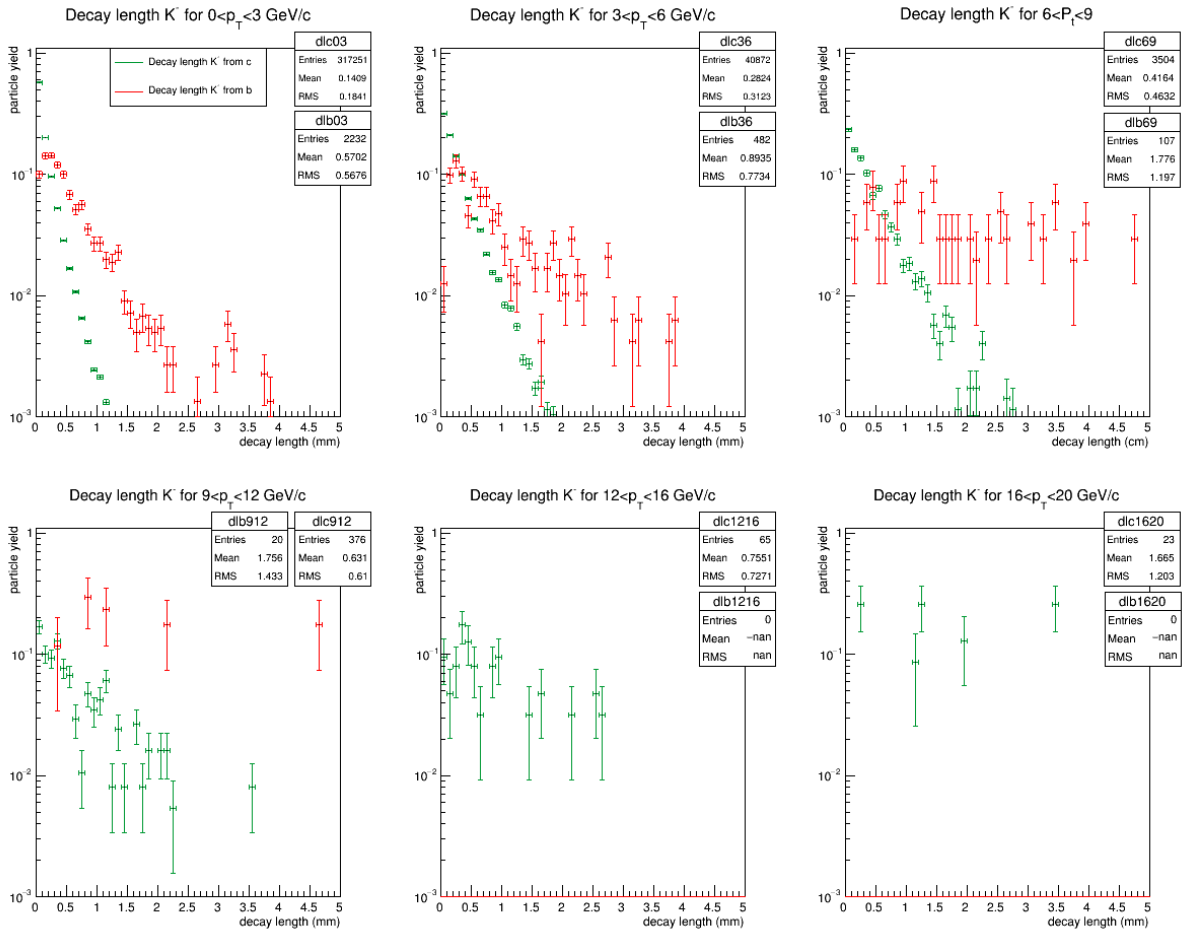

Figure 19: Decay lengths of the K^- per p_T bin. $20 * 10^6$ events, pp at 14 TeV.

The purity of kaons coming from beauty quarks has also been calculated using the data in figure 19. The purity is defined as

$$P_{K_b^-} = \frac{K_b^-}{K_b^- + K_c^-}.$$

The complete data set used can be found in Appendix B. A summary of the findings is given in table 3.

p_T **bin**	$P_{K_b^-}$ **at decay length** (μ**m**)		
	10%	**30%**	**50%**
$0 < p_T < 3$ GeV/c	1250	1950	2750
$3 < p_T < 6$ GeV/c	1350	2050	2150
$6 < p_T < 9$ GeV/c	950	1450	2350
$9 < p_T < 12$ GeV/c	850	2150	4650
$12 < p_T < 16$ GeV/c	-	-	-
$16 < p_T < 20$ GeV/c	-	-	-

Table 3: Purity of the K^- per p_T region.

In table 3, the first decay length at which a certain purity is reached is given. Therefore, it is possible that at a larger decay length, a lower purity is achieved. For example as encountered at a purity of 10% in p_T region 3 - 6: in table 11 in Appendix B it can be seen that a purity of 10.4% is achieved at a decay length of 1350 μm, while at a decay length of 1650 μm the purity drops to 2.5%. These inconsistencies contribute to the high errors in the kaon data.

Furthermore, the purity shows large fluctuations at both higher p_T bins and larger decay lengths. From p_T value 3 and up, the higher ranges of decay length show values varying from 0 to 100 per cent. This can be explained by the relatively small bin width used (100 μm). However, to enlarge the bin width would mean a larger loss of data and larger errors. An increase in statistics could be a more suitable manner to minimize these fluctuations.

Taking these factors into account, for this number of events (20 million) it would be most sensible to look in the lowest p_T region of $0 < p_T < 3$ GeV/c and make a cut at 1250 μm. This would result in sufficient data in the range of decay length 1250 and up, with an average purity of 10% or higher. A similar cut could be made in $3 < p_T < 6$ GeV/c at 1350 μm, but

the statistics minimize with a factor ~ 10 for such a p_T shift.

5 Conclusions

To obtain a clean sample of B meson decays, that is,

$$b \to B^0 \to D^{*+}\pi \to D^0\pi\pi \to K^-\pi\pi\pi,$$

some cuts in p_T regions and decay length range can be made. When focusing on the purity of the D^{*+} yield from beauty quarks, it seems sensible to make a cut at $p_T = 12$, discarding lower p_T values. This would conserve 10% of the non-prompt D^{*+} particles.

Taking the results of the decay length into account, it would be advisable to make a cut at $p_T = 6$. Within the range $6 < p_T < 9$ GeV/c, a cut at decay length 2250 μm, discarding D^{*+} decaying at a smaller distance, would result in a conservation of at least 10% in the entire p_T region $6 < p_T < 20$ GeV/c.

When the LHC runs at an energy of 14 TeV, kaons will make up for part of the particles detected. To obtain a sample of kaons where the purity of the kaons coming from beauty quarks is optimal, it would be recommended to not make a cut in p_T regions, but to make a cut in decay length. A cut at a decay length of 1250 μm results in a purity of 10% and higher in the remaining data.

5.1 Outlook

The data generated for this thesis can be used as a starting point for many further directions of research. In this section, we will give a few suggestions.

The cut in p_T region based on the purity plot seems to be a reasonable one. Discarding the lower p_T values would open the opportunity to generate data similar to that in figure 14, but with a focus on higher momentum than now has been done. With both the momentum distributions of the D^{*+} given in this research and the cut momentum distributions of the D^{*+}, the nuclear modification factor R_{AA} can be computed. To this end another simulation will have to be run, similar to the one used in figure 14, but with lead-lead collisions instead of proton-proton. The differences in R_{AA} for prompt and non-prompt D^{*+}, for cut data and data without a cut, would give insight in

the properties of a QGP.

An imaginably more promising way to compose the nuclear modification factor, is by comparing the particle yield in lead-lead collisions and proton-proton collisions based on the decay length of the D^{*+} mesons. The data in figure 18 can be used and again, simulations with lead-lead collisions at the same energy of 14 TeV would have to be run. The decay lengths of the D^{*+} produced in lead-lead collisions would have to be analyzed in a way similar to figure 18.

As can be seen in figure 18, the statistics decrease rapidly as the momentum increases. The higher the p_T region, the less entries make up for the graphs, impeding the reading of the results. Therefore, it could be worthwhile to find ways to increase these entries. The plots are based on 20 million events, which leads us to assume the statistics are sufficient. One way to achieve clearer results is to alter the settings used in PYTHIA so that the events are forced in a different way. Another method could be to decrease the size of the p_T bins. In this research bins of size $p_T = 3$ are used. Decreasing the bin size to $p_T = 2$ and simultaneously increasing the number of events to 40 million could increase the outlines of decay length distributions.

A similar argument can be made for the decay length distributions of the kaons in figure 19. In higher p_T bins the amount of information that can be abstracted from the graphs decreases drastically. Both of the methods mentioned in the previous paragraph could improve this.

When either of this measures has been used to improve the data concerning decay length, the information these simulations will provide can be displayed in an orderly way. For example, statistically decent peaks in decay length per p_T bin can be plotted in one figure, so it can be easily seen where to make the momentum cut.

References

[1] PBS NOVA, Fermilab, Office of Science, United States Department of Energy, Particle Data Group
https://commons.wikimedia.org/w/index.php?curid=4286964
10-12-2016

[2] E. Henley, A. Garcia (2007) *Subatomic Physics* World Scientific Publishing Co.

[3] M. Botje (2013) *Lecture particle physics II* Nikhef Amsterdam
http://www.nikhef.nl/~h24/qcdcourse/section-6.pdf
16-12-2016

[4] http://www.sci-news.com/physics/science-cern-littlest-quark-gluon-plasma-03206.html
20-10-2016

[5] Brookhaven National Laboratory's Relativistic Heavy Ion Collider
https://www.bnl.gov/bnlweb/pubaf/pr/photos/2012/07/RHIC_Graphics_Fig1-HR.jpg
16-10-2016

[6] Grelli, A. (2015) *Lecture on strong interactions*
http://www.staff.science.uu.nl/~grell101/StrongInt_TUM_Grelli_27Apr.pdf

[7] Edited from http://slideplayer.com/slide/8503919/, 16-12-2016
Cao S. (2011) *Dynamical Evolution, Hadronization and Angular Decorrelation of Heavy Flavor in Hot and Dense QCD Matter.* Duke University

[8] https://inspirehep.net/record/1230338/plots
19-12-2016

[9] http://aliceinfo.cern.ch/Public/en/Chapter2/Page3-ITS-en.html
20-12-2016

[10] Edited from http://slideplayer.com/slide/10789297/, 21-12-2016
Yu, W. (2016) *Particle Identification of the ALICE TPC via dE/dx.* Goethe Universität Frankfurt

[11] http://cerncourier.com/cws/article/cern/34922
21-12-2016

[12] http://home.thep.lu.se/~torbjorn/pythia81html/Welcome.html
21-12-2016

[13] https://root.cern.ch/about-root
21-12-2016

[14] Particle Data Group (2014) *Particle Physics Booklet* CERN & LBNL.

A Appendix: Tables of D^{*+} yield

For clarity reasons, the values of decay lengths that do not have any entries are left out.

DECAY LENGTH (μm)	D* PARTICLE YIELD	LEFT AFTER CUT	% OF TOTAL
50	405	1160	100
150	220	755	65.1
250	122	535	46.1
350	71	413	35.6
450	96	342	29.5
550	48	246	21.2
650	47	198	17.1
750	19	151	13.0
850	23	132	11.4
950	21	109	9.4
1050	14	88	7.6
1150	8	74	6.4
1250	20	66	5.7
1350	7	46	4.0
1550	5	39	3.4
1650	2	34	2.9
1750	4	32	2.8
1850	4	28	2.4
1950	9	24	2.1
2050	3	15	1.3
2250	3	12	1.0
2950	3	9	0.8
3050	6	6	0.5
Total	**1160**		

Table 4: Number of D* from b in p_T region $0 < p_T < 3$.

DECAY LENGTH (μm)	D* PARTICLE YIELD	LEFT AFTER CUT	% OF TOTAL
50	263	1103	100
150	221	840	76.2
250	146	619	56.1
350	93	473	43.0
450	89	380	34.5
550	47	291	26.4
650	39	244	22.1
750	45	205	18.6
850	33	160	14.5
950	9	127	11.5
1050	14	118	10.7
1150	24	104	9.4
1250	17	80	7.3
1350	12	63	5.7
1450	5	51	4.6
1550	11	46	4.2
1650	7	35	3.2
1750	3	28	2.5
1850	3	25	2.3
2050	6	22	2.0
2550	2	16	1.5
2650	3	14	1.3
2950	4	11	1.0
3050	3	7	0.6
3550	2	4	0.4
4550	2	2	0.2
Total	**1103**		

Table 5: Number of D* from b in p_T region $3 < p_T < 6$.

DECAY LENGTH (μm)	D* PARTICLE YIELD	LEFT AFTER CUT	% OF TOTAL
50	44	281	100
150	30	237	84.3
250	34	207	73.7
350	24	173	61.6
450	16	149	53.0
550	14	133	47.3
650	21	119	42.4
750	14	98	34.9
950	12	84	30.0
1050	2	72	25.6
1150	2	70	24.9
1250	4	68	24.2
1350	3	64	22.8
1450	3	61	21.7
1550	5	58	20.6
1650	9	53	18.9
1850	10	44	15.7
2050	6	34	12.1
2250	3	28	10.0
2650	6	25	8.9
2950	5	19	6.8
3050	9	14	5.0
3150	3	5	1.8
4750	2	2	0.7
Total	**281**		

Table 6: Number of D* from b in p_T region $6 < p_T < 9$.

DECAY LENGTH (μm)	D* PARTICLE YIELD	LEFT AFTER CUT	% OF TOTAL
50	9	58	100
150	3	49	84.5
250	7	46	79.3
450	6	39	67.2
950	4	33	56.9
1050	3	29	50.0
1150	3	26	44.8
1250	4	23	39.7
1350	3	19	32.8
1850	3	16	27.6
1950	2	13	22.4
2350	5	11	19.0
3450	3	6	10.3
3550	3	3	5.2
Total	**58**		

Table 7: Number of D* from b in p_T region $9 < p_T < 12$.

DECAY LENGTH (μm)	D* PARTICLE YIELD	LEFT AFTER CUT	% OF TOTAL
150	5	30	100
250	2	25	83.3
450	4	23	76.7
1350	3	19	63.3
1650	2	16	53.3
2650	4	14	46.7
3250	3	10	33.3
3850	4	7	23.3
4350	3	3	10.0
Total	**30**		

Table 8: Number of D* from b in p_T region $12 < p_T < 16$.

DECAY LENGTH (μm)	D* PARTICLE YIELD	LEFT AFTER CUT	PERCENTAGE %
150	3	11	100
250	3	8	72.7
550	2	5	45.5
2750	3	3	27.3
Total	**11**		

Table 9: Number of D* from b in p_T region $16 < p_T < 20$.

B Appendix: Tables of K^- yield

For clarity reasons, the values of decay lengths that do not have any entries are left out.

DECAY LENGTH (μm)	K_c^-	K_b^-	PURITY $P_{K_b^-}$ (%)
50	182312	223	0.1
150	63812	316	0.5
250	30429	320	1.0
350	16661	268	1.6
450	9094	223	2.4
550	5302	151	2.8
650	3389	115	3.3
750	2059	125	5.7
850	1322	79	5.6
950	779	60	7.2
1050	676	60	8.2
1150	419	44	9.5
1250	261	42	13.9
1350	200	51	20.3
1450	162	20	11.0
1550	97	16	14.2
1650	59	11	15.7
1750	48	15	23.8
1850	64	12	15.8
1950	19	11	36.7
2050	22	12	35.3
2150	11	6	35.3
2250	12	6	33.3
2350	10	2	16.7
2450	4	0	0
2550	5	0	0
2650	5	3	37.5
2750	0	2	100
2950	0	6	100
3150	5	13	72.2
3250	3	8	61.5
3750	2	5	71.4
3850	2	3	60.0
4150	6	0	0
5050	0	4	100
Total	**317251**	**2232**	**0.7%**

Table 10: Number of K_{45}^-in p_T region $0 < p_T < 3$.

DECAY LENGTH (μm)	K_c^-	K_b^-	PURITY $P_{K_b^-}$ (%)
50	12994	6	0.1
150	8618	48	0.6
250	5798	62	1.1
350	4081	49	1.2
450	2612	22	0.8
550	1768	44	2.4
650	1411	32	2.2
750	904	32	3.4
850	639	20	3.0
950	554	23	4.0
1050	342	12	3.4
1150	320	7	2.1
1250	227	6	2.6
1350	121	14	10.4
1450	112	13	10.4
1550	70	8	10.3
1650	79	2	2.5
1750	47	8	14.6
1850	43	13	23.2
1950	27	7	20.6
2050	26	5	16.1
2150	14	14	50.0
2250	15	7	31.8
2350	14	5	26.3
2450	3	0	0
2550	6	0	0
2650	0	0	0
2750	8	10	55.6
2850	2	3	60
3150	0	2	100
3250	0	3	100
3650	8	0	0
3750	0	2	100
3850	0	3	100
Total	**40872**	**482**	**1.2%**

Table 11: Number of K^- in p_T region $3 < p_T < 6$.

DECAY LENGTH (μm)	K_c^-	K_b^-	PURITY $P_{K_b^-}$ (%)
50	817	0	0
150	563	3	0.5
250	479	0	0
350	359	6	1.6
450	235	8	3.3
550	268	3	1.1
650	163	3	1.8
750	129	0	0
850	102	6	5.6
950	62	9	12.7
1050	64	0	0
1150	46	0	0
1250	48	5	9.4
1350	37	0	0
1450	20	9	31
1550	14	3	17.7
1650	24	3	11.1
1750	19	3	13.6
1850	4	3	42.9
2050	6	3	33.3
2150	6	2	25.0
2250	14	0	0
2350	3	3	50.0
2450	3	0	0
2550	0	5	100
2650	5	3	37.5
2750	4	0	0
3050	0	4	100
3250	2	3	60.0
3750	3	2	40.0
3850	2	0	0
3950	0	4	100
4750	0	3	100
4950	3	0	0
5050	0	5	100
Total	**3504**	**107**	**3.0%**

Table 12: Number of K_b^- in p_T region $6 < p_T < 9$.

DECAY LENGTH (μm)	K_c^-	K_b^-	PURITY $P_{K_b^-}$ (%)
50	64	0	0
150	38	0	0
250	35	0	0
350	49	2	3.9
450	29	0	0
550	25	0	0
650	11	0	0
750	4	0	0
850	18	5	21.7
950	13	0	0
1050	16	0	0
1150	23	4	14.8
1250	3	0	0
1350	9	0	0
1450	3	0	0
1650	10	0	0
1750	3	0	0
1850	6	0	0
2050	6	0	0
2150	6	3	33.3
2250	2	0	0
3550	3	0	0
4650	0	3	100
5050	0	3	100
Total	**367**	**20**	**5.2%**

Table 13: Number of K^- in p_T region $9 < p_T < 12$.

DECAY LENGTH (μm)	K_c^-	K_b^-	PURITY $P_{K_b^-}$ (%)
50	6	0	0
150	3	0	0
250	5	0	0
350	11	0	0
450	8	0	0
550	5	0	0
650	2	0	0
750	0	0	0
850	5	0	0
950	6	0	0
1450	2	0	0
1650	3	0	0
2150	2	0	0
2550	3	0	0
2650	2	0	0
5050	2	0	0
Total	**65**	**0**	**0%**

Table 14: Number of K^- in p_T region $12 < p_T < 16$.

DECAY LENGTH (μm)	K_c^-	K_b^-	PURITY $P_{K_b^-}$ (%)
250	6	0	0
1150	2	0	0
1250	6	0	0
1950	3	0	0
3450	6	0	0
Total	**23**	**0**	**0%**

Table 15: Number of K^- in p_T region $16 < p_T < 20$.